

Skyrmion motion induced by spin-waves on magnetic nanotubes

Tijjani Abdulrazak, Xuejuan Liu(刘雪娟), Zhenyu Wang(王振宇), Yunshan Cao(曹云姗), and Peng Yan(严鹏)
Citation: Chin. Phys. B, 2024, 33 (**10**): 107504. DOI: 10.1088/1674-1056/ad5d64
Journal homepage: http://cpb.iphy.ac.cn; http://iopscience.iop.org/cpb

What follows is a list of articles you may be interested in

Simulation of magnetization process and Faraday effect of magnetic bilayer films

Sheng Gao(高升), An Du(杜安), Lei Zhang(张磊), Tian-Guang Li(李天广), and Da-Cheng Ma(马大成)
Chin. Phys. B, 2024, 33 (**9**): 097505. DOI: 10.1088/1674-1056/ad5a76

Magnetic domain structures in ultrathin $Bi_2Te_3/CrTe_2$ heterostructures

Tirui Xia(夏体瑞), Xiaotian Yang(杨笑天), Yifan Zhang(张逸凡), Xinqi Liu(刘馨琪), Xinyu Cai(蔡新雨), Chang Liu(刘畅), Qi Yao(姚岐), Xufeng Kou(寇煦丰), and Wenbo Wang(王文波)
Chin. Phys. B, 2024, 33 (**8**): 087504. DOI: 10.1088/1674-1056/ad4a3a

Evolution of anomalous Hall effect in ferromagnetic Weyl semimetal $Nb_xZr_{1-x}Co_2Sn$

Bo-Wen Chen(陈博文) and Bing Shen(沈冰)
Chin. Phys. B, 2024, 33 (**8**): 087501. DOI: 10.1088/1674-1056/ad4a3b

Critical behavior of quasi-two-dimensional ferromagnet $Cr_{1.04}Te_2$

Wei Niu(钮伟), Qin-Xin Song(宋沁心), Shi-Qi Chang(常世琦), Min Wang(王敏), Kui Yuan(袁奎), Jia-Cheng Gao(高嘉程), Shuo Wang(王硕), Zhen-Dong Wang(王振东), Kai-Fei Liu(刘凯斐), Ping Liu(刘萍), Yong-Bing Xu(徐永兵), Xiao-Qian Zhang(张晓倩), and Yong Pu(普勇)
Chin. Phys. B, 2024, 33 (**7**): 077506. DOI: 10.1088/1674-1056/ad4cd8

Relationship between disorder, magnetism and band topology in $Mn(Sb_{1-x}Bi_x)_2Te_4$ single crystals

Ming Xi(席明) and Hechang Lei(雷和畅)
Chin. Phys. B, 2024, 33 (**6**): 067503. DOI: 10.1088/1674-1056/ad3dd8

Skyrmion motion induced by spin-waves on magnetic nanotubes

Tijjani Abdulrazak[1,2,‡], Xuejuan Liu(刘雪娟)[1,3], Zhenyu Wang(王振宇)[1], Yunshan Cao(曹云姗)[1], and Peng Yan(严鹏)[1,†]

[1] *School of Physics and State Key Laboratory of Electronic Thin Films and Integrated Devices, University of Electronic Science and Technology of China, Chengdu* 610054, *China*
[2] *Department of Physics, Bayero University, Kano*-700006, *Nigeria*
[3] *School of Healthcare Technology, Chengdu Neusoft University, Chengdu* 611844, *China*

(Received 17 December 2023; revised manuscript received 22 June 2024; accepted manuscript online 1 July 2024)

We investigate the skyrmion motion driven by spin waves on magnetic nanotubes through micromagnetic simulations. Our key results include demonstrating the stability and enhanced mobility of skyrmions on the edgeless nanotube geometry, which prevents destruction at boundaries — a common issue in planar geometries. We explore the influence of the damping coefficient, amplitude, and frequency of microwaves on skyrmion dynamics, revealing a non-uniform velocity profile characterized by acceleration and deceleration phases. Our results show that the skyrmion Hall effect is significantly modulated on nanotubes compared to planar models, with specific dependencies on the spin-wave parameters. These findings provide insights into skyrmion manipulation for spintronic applications, highlighting the potential for high-speed and efficient information transport in magnonic devices.

Keywords: ferromagnetic, magnetic nanotube, Mumax3 software, skyrmion, spin-wave

PACS: 75.50.Gg, 71.35.Ji, 12.39.Dc, 75.30.Ds **DOI:** 10.1088/1674-1056/ad5d64

1. Introduction

Magnetic skyrmions are safeguarded topological spin textures which were noted in experiments within a thin magnetic film or chiral bulk.[1–3] They are anticipated to serve as the perfect communication carriers in the next generation of spintronic gadgets due to their compact size, excellent thermal stability, and low driving current for motion.[4,5] Reliable skyrmion motion manipulation is crucial for information-processing applications.[6] Prior research on the dynamic motions of skyrmions was mainly concerned with two-dimensional (2D) planar geometry, such as nanodisks, thin films, and nanostripes.[7–11,11] Unfortunately, information will be lost at the track boundary due to skyrmions building up or annihilating due to the skyrmion Hall effect.[12–14] Several methods have been suggested as solutions to this issue, including suppressing the skyrmion Hall effect by turning magnetic parameters[15–19] or modifying magnetic structures[20,21] at the film edge and eliminating the topological charge by an antiferromagnetically exchange-coupled bilayer skyrmion,[22] antiferromagnetic skyrmion,[23,24] skyrmionium,[25] or introducing new functionality;[26,27] but this is tricky to be realized in experiments.[14,28] Researchers now focus on nanostructures having circular cross-sections, e.g., magnetic spheres or cylinders. The skyrmion motion on boundary-free samples would be a desirable direction of research, and magnetic nanotubes constitute a promising option because the nanotube has no boundary in the tangent direction, so the skyrmions cannot disappear at the boundary.

Recently, Wang *et al*. studied the electrical current-driven motion of skyrmions in magnetic nanotubes,[29] demonstrating that the skyrmions moving on the magnetic nanotube avoid the information loss brought about by destroying the skyrmions at the boundary and moving faster. Xin and Liu considered a rotating magnetic field to drive the motion of a skyrmion in a nanotube and studied its skyrmion Hall effects.[30] It was found that the strength of the skyrmion Hall effect is related to the size of the nanotube, the frequency of the rotating magnetic field, and the Gilbert damping coefficient. All these simulation results prove the significance of the research on magnetic nanotubes. On the other hand, Joule heating, due to the high current density, is a bottleneck for spintronic applications based on electron spin currents. The spin wave (SW) provides a promising possibility for controlling a skyrmion without the Joule heating, in principle.[9,31]

This study focuses on the skyrmion motion induced by SWs on magnetic nanotubes. This geometry offers boundary-free motion and enhanced stability, which the literature has yet to explore extensively. We investigate how varying the damping coefficient, SW amplitude, and frequency affects the skyrmion velocity and the skyrmion Hall effect. Our key findings are as follows: the skyrmion velocity decreases as the damping coefficient increases; there is more stability and reduction in computational load of the skyrmion at a high damping coefficient; a SW propelling skyrmion can exhibit a spiral motion because the tube geometry is edgeless; and finally, when compared to the planar model, the magnetic nanotube

†Corresponding author. E-mail: yan@uestc.edu.cn
‡Corresponding author. E-mail: atijjani.phy@buk.edu.ng

© 2024 Chinese Physical Society and IOP Publishing Ltd

can well modify the skyrmion Hall effect.

2. Model and micromagnetic simulation details

Our model consists of a set of geometry (nanotubes) with a fixed thickness ($d = 20$ nm, 30 nm inner radius), length ($L = 600$ nm), and outer radius ($R = 50$ nm), as shown in Fig. 1. The Mumax3 software package was utilized to conduct the micromagnetic simulations to examine the motions of a skyrmion produced by an SW on magnetic nanotubes.[32] The magnetization distribution evolves according to the Landau–Lifshitz–Gilbert (LLG) equation, which is expressed as

$$\frac{\partial \boldsymbol{m}}{\partial t} = -\gamma \boldsymbol{m} \times \boldsymbol{H}_{\text{eff}} + \alpha \boldsymbol{m} \times \frac{\partial \boldsymbol{m}}{\partial t}, \tag{1}$$

where γ is the gyromagnetic ratio, $\boldsymbol{m}$ is the unit vector of the magnetization, $\boldsymbol{H}_{\text{eff}} = -\frac{1}{M_s}\frac{\delta \varepsilon}{\delta \boldsymbol{m}}$ is the effective field, M_s is the saturation magnetization, ε is the energy density, and α is the Gilbert damping parameter. In this proposed system, the total energy density of the magnetic system reads

$$\varepsilon = A_{\text{ex}}(\nabla \boldsymbol{m})^2 + D\boldsymbol{m} \cdot (\nabla \times \boldsymbol{m}) - K(\boldsymbol{m} \cdot \hat{\rho})^2 + E_{\text{DDI}}, \tag{2}$$

where A_{ex} is the exchange stiffness, D is the bulk Dzyaloshinskii–Moriya interaction (DMI) strength, $K > 0$ is the easy-normal anisotropy parameter along the $\hat{\rho}$ axis (normal direction), and E_{DDI} is the energy density of the dipole–dipole interaction. The dipole–dipole exchange is included in numerical simulations, and the parameters for the FeGe[33] material used are exchange constant $A_{\text{ex}} = 8.78$ pJ/m, saturation magnetization $M_s = 2 \times 10^5$ A/m, bulk DMI parameter $D = 1$ mJ/m^2, and easy-normal anisotropy constant $K_\rho = 2 \times 10^5$ J/m^3. We employed absorbing boundary conditions at the endpoints of the nanotubes to inhibit SW reflection.[34] These boundary conditions effectively dampen outgoing SWs, preventing them from bouncing back and interfering with the simulated dynamics. The stabilization of the skyrmion spin texture is illustrated in Fig. 1, where the middle represents the nanotube axis center and the selected coordinate. A scheme describing the skyrmion center is displayed in the inset. The red color refers to the magnetization's orientation along the positive ρ-direction, and the blue color refers to the magnetization being oriented along the negative ρ-direction. The center position of the skyrmion is defined as (R_φ, R_z)[35] according to the guiding and geometric center of the core, respectively,

$$R_\varphi = \frac{\int \varphi q \, \mathrm{d}\varphi \, \mathrm{d}z}{\int q \, \mathrm{d}\varphi \, \mathrm{d}z}, \quad R_z = \frac{\int z q \, \mathrm{d}\varphi \, \mathrm{d}z}{\int q \, \mathrm{d}\varphi \, \mathrm{d}z}. \tag{3}$$

The topological density is given by $q = \boldsymbol{m} \cdot \left(\frac{\partial \boldsymbol{m}}{\partial x} \times \frac{\partial \boldsymbol{m}}{\partial y}\right)$.[35] This research was built upon the previous work conducted in Ref. [29], which provided an in-depth description of the characteristics of an ordinary isolated skyrmion. The simulation results obtained in this study underscore the nanotube's research significance.

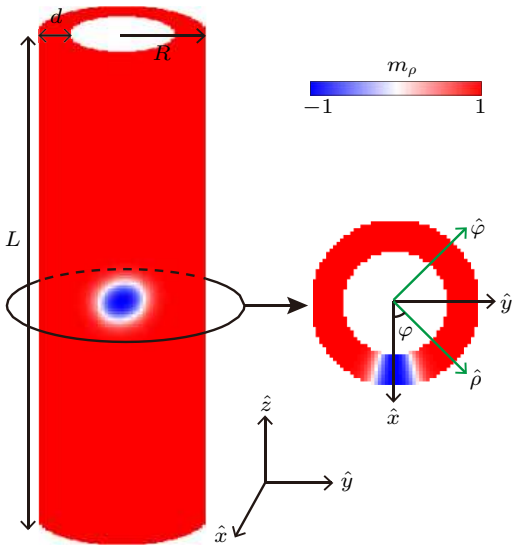


Fig. 1. Diagrammatic representation of a Bloch-type skyrmion stabilized on a magnetic nanotube, where R and d represent the outer radius and thickness, respectively. The origin is the center of the tube, and $\hat{\rho}$, $\hat{\phi}$, and $\hat{z}$ represent the radial azimuthal, and axial directions, respectively. For the analytical investigation, cylindrical and Cartesian coordinates are employed.

3. Results and discussion

After ensuring that the skyrmion is stable, as presented in Fig. 1, a sinusoidal monochromatic microwave $\boldsymbol{H}_{\text{ex}} = h_0 \sin(\omega t)\hat{z}$ is applied along the $\hat{z}$-axis at $z < -135$ nm below the position of the skyrmion, with $h_0 = 100$ mT and $\omega/(2\pi) = 60$ GHz, where h_0 and ω are the field amplitude and the angular frequency, respectively. When SWs reach the excitation region, they propagate on magnetic nanotubes, and drive the skyrmion motion along two directions. The first one measures the displacement (z) along a perpendicular direction, while the other one is the angular displacement (φ) along a parallel direction. The skyrmion's velocity is composed of two parts: $v_\perp$ and $v_\parallel$, where $v_\perp = \mathrm{d}z/\mathrm{d}t$ is the velocity along a perpendicular direction and $v_\parallel = r\mathrm{d}\varphi/\mathrm{d}t$ is the velocity along a parallel direction. First, we analyze the influence of damping coefficient α on the skyrmion velocity by altering the damping coefficient from 0.01 to 0.05 with a step interval of 0.01 as the damping coefficient plays a crucial role in regulating the behavior of skyrmion movement.

We unroll the m_ρ image of the nanotube depicted in Fig. 1 onto a planar φ–z plane, as illustrated in Fig. 2, where the magnetization is normalized to $m_z = 0$ for more convenience. Upon setting the damping coefficient to 0.01, as depicted in Fig. 2(a), we observe intriguing dynamics: the skyrmion exhibits perpendicular and parallel velocities of 4.99 m·s^{-1} and 0.72 m·s^{-1}, respectively, after traveling a distance of 155.12 nm along the z direction and $-2.69°$ along the φ direction on the nanotube for 20 ns. However, the mobility of the skyrmion notably decreases when the damping coefficient is raised to 0.02, as shown in Fig. 2(b). Under this condition,

it only manages to move a distance of 93.18 nm along the z direction and $-2.79°$ along the φ direction, maintaining perpendicular and parallel velocities of 3.77 $\mathrm{m\cdot s^{-1}}$ and 0.103 $\mathrm{m\cdot s^{-1}}$, respectively.

Further increasing the damping coefficient to 0.05, as depicted in Fig. 2(c), leads to a significant decrease in the skyrmion's mobility. At $t = 20$ ns, the skyrmion barely progresses, covering a mere 14.39 nm along the z direction and $-2.23°$ along the φ direction, with perpendicular and parallel velocities of 0.69 $\mathrm{m\cdot s^{-1}}$ and -0.02 $\mathrm{m\cdot s^{-1}}$, respectively. This observation underscores the strong correlation between the damping coefficient and the skyrmion's mobility. As the damping coefficient rises, the efficiency of the skyrmion's movement is compromised because the excited SW decays quickly as the damping coefficient increases, causing its amplitude to decrease. The damping coefficient for SW-driven skyrmions is kept constant at 0.01 throughout the work to achieve better simulation results.

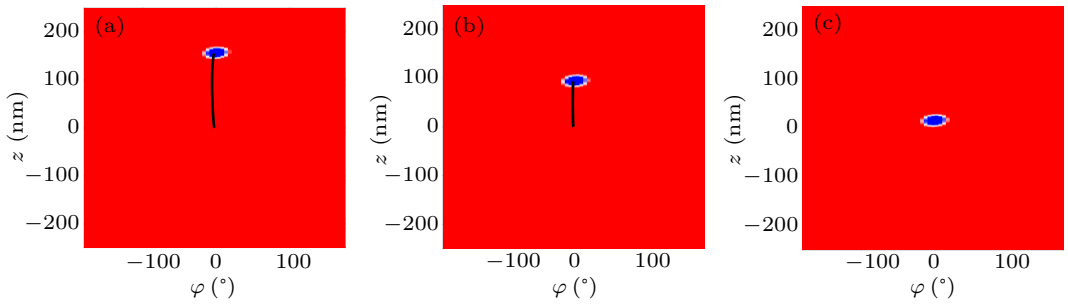


Fig. 2. Image of the propagation of a skyrmion induced by SWs on the middle layer of magnetic nanotubes under different damping coefficients with $\omega/(2\pi) = 60$ GHz, $h_0 = 100$ mT and $t = 20$ ns. The black curve represents the path of the skyrmion motion. (a) Damping coefficient of 0.01. (b) Damping coefficient of 0.02. (c) Damping coefficient of 0.05.

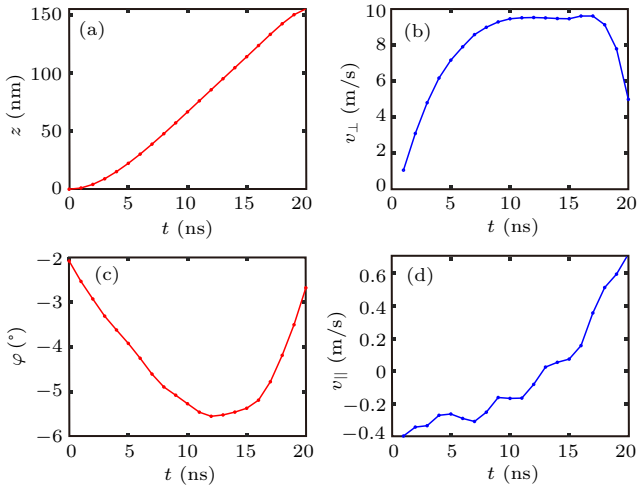


Fig. 3. Skyrmion motion induced by a SW with $\omega/(2\pi) = 60$ GHz, $h_0 = 100$ mT, and $t = 20$ ns within the nanotubes. (a) Displacement of skyrmion motion along the z direction with time, (b) skyrmion velocity along the z direction with time, (c) angular displacement of skyrmion motion along the φ direction with time, (d) skyrmion velocity with time.

Figure 3 shows the skyrmion's displacement and velocity as a function of time for $R = 50$ nm, $d = 20$ nm, $\alpha = 0.01$, $\omega/(2\pi) = 60$ GHz, and $h_0 = 100$ mT; the skyrmion's velocity is not uniform and experiences acceleration and deceleration. In Fig. 3(a), the displacement of skyrmion motion along the z direction increases with time; while in Fig. 3(b), the skyrmion's velocity is not uniform. During the first 17 ns, the maximal velocity is ~ 9.61 $\mathrm{m\cdot s^{-1}}$ and the average velocity is ~ 7.76 $\mathrm{m\cdot s^{-1}}$ for the entire time. Figure 3(c) shows the angular displacement of the skyrmion motion along the φ direction; the angular displacement φ increases and attains a maximum of $-5.54°$ along the φ direction in 12 ns, and later increases up to $-2.69°$ for 20 ns. Figure 3(d) shows the skyrmion velocity along the parallel direction; the velocity increases with time.

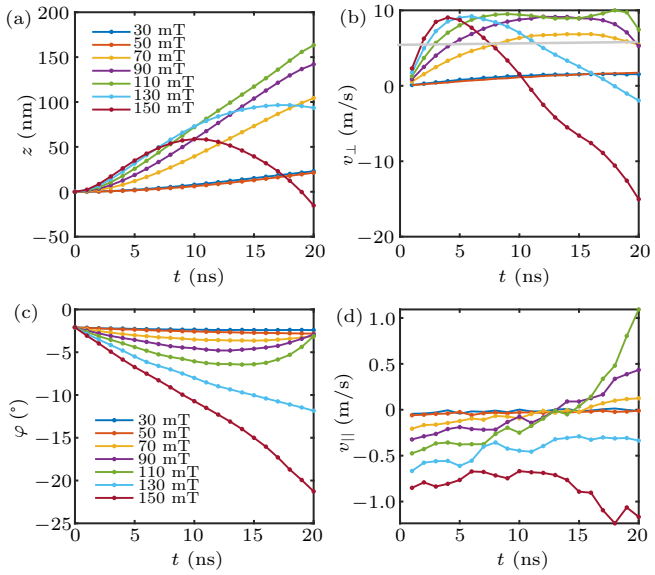


Fig. 4. Skyrmion motion induced by SWs under different amplitudes with $\omega/(2\pi) = 60$ GHz on the nanotubes. (a) Displacement of the skyrmion along the z direction with time, (b) skyrmion velocity along the z direction with time. The gray line represents the critical velocity of the skyrmion motion. (c) Angular displacement of skyrmion motion along the φ direction with time, (d) skyrmion velocity along the $v_{\parallel}$ direction with time.

The displacement and velocity of the skyrmion as a function of time for $R = 50$ nm, $d = 20$ nm, $\alpha = 0.01$, and $\omega/(2\pi) = 60$ GHz when varying the amplitude of the magnetic field are presented in Fig. 4. Notably, it is found that a more substantial increase in the amplitude of the magnetic field leads to an increase in the skyrmion's displacement and velocity as time increases. Figure 4(a) shows the displacement of the skyrmion along the z direction with time; the displacement increases with an increase in time for an amplitude below 110 mT, while for an amplitude of 130 mT the displacement

decreases at 19 ns, and for an amplitude of 150 mT at time 11 ns the displacement decreases drastically. The skyrmion velocity along the perpendicular direction with time is depicted in Fig. 4(b), where a larger amplitude leads the larger maximal/average velocity. But for amplitudes 130 mT and 150 mT, the skyrmion's velocity decelerates at some point. The gray line in Fig. 4(b) shows the critical velocity of the skyrmion motion. Figure 4(c) shows the angular displacement of skyrmion motion along the φ direction with time; the magnitude of the angular displacement of the skyrmion increases as the time increases. Figure 4(d) shows the skyrmion velocity along the parallel direction with time.

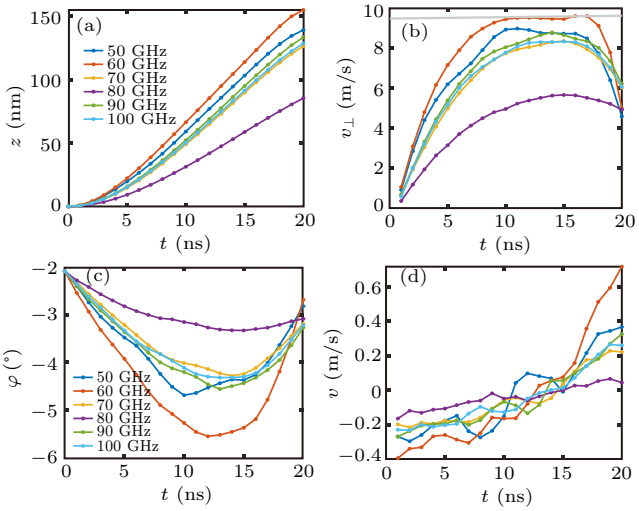


Fig. 5. Skyrmion motion induced by SW under different frequencies with $h_0 = 100$ mT, $\alpha = 0.01$, $d = 20$ nm, $R = 50$ nm and $t = 20$ ns on the nanotubes. (a) Displacement of skyrmion motion along the z direction with time, (b) skyrmion velocity along the z direction with time. The gray line represents the maximum velocity of the skyrmion motion. (c) Angular displacement of skyrmion motion along the φ direction with time, (d) skyrmion velocity with time.

Figure 5 illustrates the skyrmion motion induced by SWs under different magnetic field frequencies with $h_0 = 100$ mT, $\alpha = 0.01$, $d = 20$ nm, $R = 50$ nm and $t = 20$ ns on the nanotubes. It is found that a more substantial increase in the magnetic field frequency leads to increased displacement and velocity of the skyrmion as time increases. Figure 5(a) shows the displacement of skyrmion motion along the z direction with time; the displacement increases with the time and the maximum displacement is at 60 GHz, while Fig. 5(b) shows the skyrmion velocity along the perpendicular direction with time. Initially, the skyrmion experiences an acceleration phase, followed by a decrease in its velocity. The skyrmion propagates when an SW passes through it because of strong interactions between the incoming SW and the skyrmion, which produce a reactive torque. During the hastening phase, the SW is impeded by the presence of skyrmions, resulting in an increased transfer of torque from the SW to the skyrmions and, consequently, an increase in the skyrmion's velocity. After a sufficient time, the skyrmion gradually moves away from the region where it was initially excited, and its velocity decreases as the SW diminishes. The gray line shown in Fig. 5(b) represents the critical velocity of the skyrmion motion, and the maximum velocity occurs at an optimum frequency of 60 GHz. Figure 5(c) shows the angular displacement of skyrmion motion along the φ direction with time; the angular displacement of the skyrmion decreases as time increases. Figure 5(d) shows the skyrmion velocity along the parallel direction with time; the velocity increases with an increase in time.

Furthermore, the average velocity of skyrmions was obtained for different damping coefficient (α), amplitude and frequency along the perpendicular and parallel directions, respectively. Next, we explore the influence of damping coefficient (α), amplitude and frequency on the average velocity to determine the skyrmion Hall angle and compare our results with other works. We study the effect of α on $\bar{v}_\perp$ and $\bar{v}_\parallel$ for $R = 50$ nm, $d = 20$ nm, $\omega/(2\pi) = 60$ GHz, and $h_0 = 100$ mT. Figure 6(a) shows the skyrmion trajectories along z and ρ under different α. Figure 6(b) illustrates the relationship between skyrmion $\bar{v}_\perp$ and α parameter. The results show that $\bar{v}_\perp$ is inversely proportional to α (when $\alpha = 0.01$, $\bar{v}_\perp = 7.8\ \mathrm{m\cdot s^{-1}}$ and when $\alpha = 0.05$, $\bar{v}_\perp = 0.72\ \mathrm{m\cdot s^{-1}}$). Figure 6(c) illustrates the relationship between skyrmion velocity $\bar{v}_\parallel$ and α parameter. The results show that the skyrmion on the magnetic nanotube with higher damping coefficient (α) has a smaller $\bar{v}_\parallel$ (when $\alpha = 0.01$, $\bar{v}_\parallel = -0.025\ \mathrm{m\cdot s^{-1}}$ and when $\alpha = 0.05$, $\bar{v}_\parallel = -0.0057\ \mathrm{m\cdot s^{-1}}$). The relationship is non-linear.

We study the effect of the amplitude of the microwave field on $\bar{v}_\perp$ and $\bar{v}_\parallel$ for $R = 50$ nm, $d = 20$ nm, $\omega/(2\pi) = 60$ GHz, and $\alpha = 0.01$. Figure 7(a) shows the skyrmion trajectories along z and ρ under different amplitudes of the microwave field. Figure 7(b) illustrates the relationship between $\bar{v}_\perp$ and the amplitude of the microwave field. The results show that $\bar{v}_\perp$ increases with the increase of the amplitude and attains a maximum $8.2\ \mathrm{m\cdot s^{-1}}$ at an amplitude of 110 mT. Above the amplitude of 110 mT, the $\bar{v}_\perp$ decreases. Figure 7(c) illustrates the relationship between $\bar{v}_\parallel$ and the amplitude of the microwave field. The results show that the skyrmion velocity is nearly the same but drastically decreases for amplitudes beyond 110 mT.

Finally, we study the effect of microwave frequency on $\bar{v}_\perp$ and $\bar{v}_\parallel$ for $R = 50$ nm, $d = 20$ nm, $h_0 = 100$ mT, and $\alpha = 0.01$. Figure 8(a) shows the skyrmion trajectories along z and ρ under different driving frequencies. Figure 8(b) shows the relationship between $\bar{v}_\perp$ and the driving frequency. The results show that the maximum $\bar{v}_\perp$ is $7.76\ \mathrm{m\cdot s^{-1}}$ at 60 GHz and the relationship is non-linear. Figure 8(c) illustrates the relationship between $\bar{v}_\parallel$ and the driving frequency. The results show that $\bar{v}_\parallel$ is a non-linear function of the frequency and it attains $\bar{v}_\parallel = -0.025$ at 60 GHz.

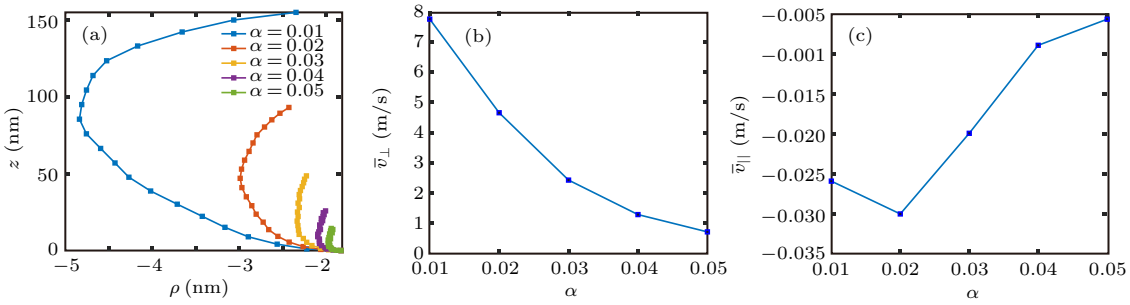


Fig. 6. (a) Skyrmion trajectories along z and ρ under different α. (b), (c) Relationship between skyrmion velocities and damping parameter. In the simulations, we set $h_0 = 100$ mT, $R = 50$ nm, $d = 20$ nm, and $\omega/(2\pi) = 60$ GHz for 20 ns.

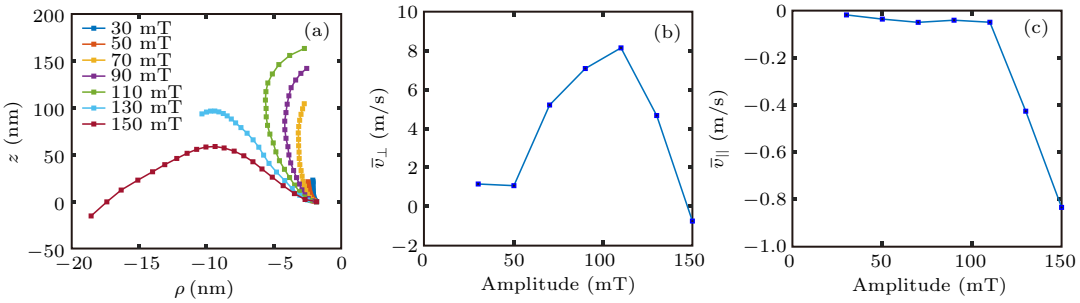


Fig. 7. (a) Skyrmion trajectories along z and ρ under different amplitudes of the microwave field. (b), (c) Relationship between skyrmion velocities and the amplitude of the microwave field. In the simulation, we set $\alpha = 0.01$, $R = 50$ nm, $d = 20$ nm, and $\omega/(2\pi) = 60$ GHz for 20 ns.

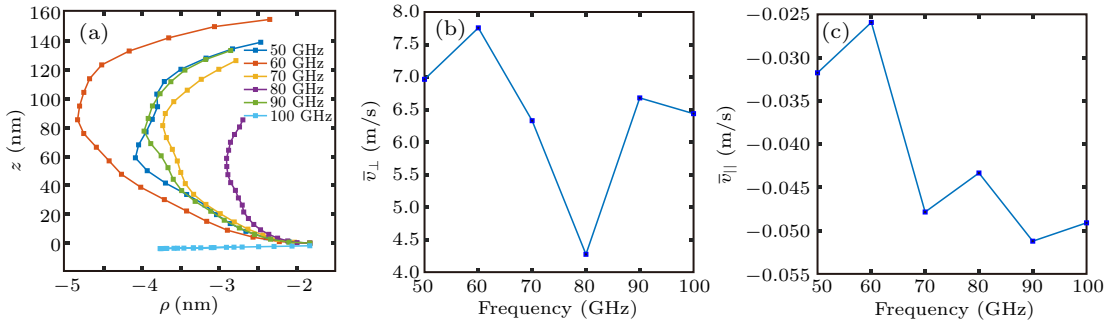


Fig. 8. (a) Skyrmion trajectories along z and ρ under different driving frequencies. (b), (c) Relationship between skyrmion velocities and driving frequency. In the simulation, we set $\alpha = 0.01$, $R = 50$ nm, $d = 20$ nm, and $h_0 = 100$ mT for 20 ns.

The variation of skyrmion Hall angle (θ_{SHA}) defined as $\theta_{\mathrm{SHA}} = \arctan\left(\bar{v}_\parallel/\bar{v}_\perp\right)$ is shown in Fig. 9. Figures 9(a) and 9(c) show that the magnitude θ_{SHA} is small when we vary the damping coefficient (α) and the microwave frequency. In Fig. 9(b), we observe a drastic change in θ_{SHA} when the amplitude of the microwave field goes beyond 110 mT. The θ_{SHA} is 5.2° with the magnitude of the skyrmion velocity ratio $\bar{v}_\parallel/\bar{v}_\perp = 0.09$ for amplitude 130 mT, and θ_{SHA} is 47.6° with the magnitude of the skyrmion velocity ratio $\bar{v}_\parallel/\bar{v}_\perp = 1.09$ for amplitude 150 mT.

We compare our results with those from the planar model and those describing skyrmion motion driven by a rotating magnetic field in nanotubes under various conditions. When a current drives skyrmions, the ratio of the in-plane velocity components is $v_y/v_x \approx 6$.[36] In thin films, when a temperature gradient drives the skyrmions, the magnitude of the skyrmion Hall effect is $v_y/v_x \approx 0.16$.[37] Additionally, when driven by voltage-controlled magnetic anisotropy, simulations indicate a ratio of $v_y/v_x \approx 7$.[38] Moreover, the magnitude of the skyrmion Hall effect reaches 10.35 when a rotating magnetic field drives skyrmion motion in nanotubes.[30] In contrast, skyrmion motion induced by spin waves in magnetic nanotubes shows that the skyrmion's velocity is not uniform and the magnitude of the skyrmion Hall effect reaches 0.09 for amplitude 130 mT and 1.09 for amplitude 150 mT, under damping coefficient $\alpha = 0.01$. The damping coefficient, amplitude, and frequency of SWs significantly influence the dynamics of skyrmion motion. Skyrmion motion induced by SWs on magnetic nanotubes offers several significant advantages over traditional methods, including energy efficiency due to the absence of Joule heating, improved stability from the edgeless nanotube geometry, and the potential for magnetic field-free operation. These features, combined with the enhanced control over skyrmion dynamics, make this approach highly promising for developing future spintronic devices.

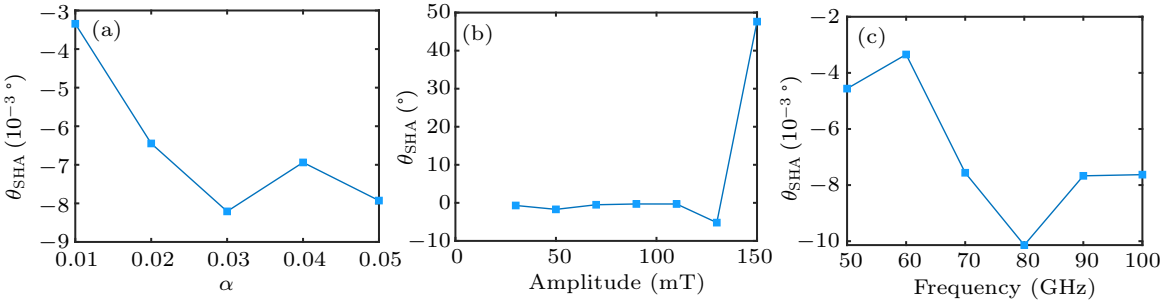


Fig. 9. (a) Magnitude $\theta_{\rm SHA}$ as a function of the damping α parameter for $R = 50$ nm, $d = 20$ nm, $\omega/(2\pi) = 60$ GHz, and $h_0 = 100$ mT. (b) Magnitude $\theta_{\rm SHA}$ as a function of the microwave amplitude for $R = 50$ nm, $d = 20$ nm, $\omega/(2\pi) = 60$ GHz, and $\alpha = 0.01$. (c) Magnitude $\theta_{\rm SHA}$ as a function of microwave frequency for $R = 50$ nm, $d = 20$ nm, $h_0 = 100$ mT, and $\alpha = 0.01$.

4. Conclusion and perspectives

In conclusion, the skyrmion motion induced by SWs on magnetic nanotubes has been systematically investigated through micromagnetic simulations. We find that skyrmions driven by SWs exhibit trajectory motion in edgeless tube geometries, mitigating Joule heating effects from high current densities. The non-linear relationship between damping and skyrmion velocity, influenced by SW frequencies, offers significant control over skyrmion manipulation. Increasing the SW frequency enhances the skyrmion velocity, with an optimum frequency of 60 GHz resulting in maximum velocities of 9.6 $\rm m\cdot s^{-1}$ in the perpendicular direction and 0.72 $\rm m\cdot s^{-1}$ in the parallel direction. Higher amplitudes of driving SWs increase the skyrmion velocity and performance in magnonic devices, although extremely high amplitudes may cause distortions and nonlinear effects. The nanotube geometry modifies the skyrmion Hall effect compared to both planar models and rotating magnetic fields. The Hall angle remains stable across varying damping coefficients and frequencies but changes with magnetic field amplitudes above 110 mT. All these findings underscore the potential for precise control of skyrmion motion by adjusting the damping coefficient, amplitude, and frequency of SWs, which is crucial for high-speed and efficient magnonic applications. Future research should explore the effects of additional external parameters, such as temperature, and investigate various magnetic nanotube geometries and materials to uncover new phenomena and expand the application scope.

Acknowledgements

This project was supported by the National Key R&D Program of China (Grant No. 2022YFA1402802) and the National Natural Science Foundation of China (Grant Nos. 12434003, 12374103, and 12074057). Tijjani acknowledges the helpful discussions with Dr. Zhejunyu Jin, Mr. Zhaozhuo Zeng and Dr. Huanhuan Yang.

References

[1] Muhlbauer S, Binz B, Jonietz F, Pfleiderer C, Rosch A, Neubauer A, Georgii R and Boni P 2009 *Science* **323** 915
[2] Yu X Z, Onose Y, Kanazawa N, Park J H, Han J H, Matsui Y, Nagaosa N and Tokura Y 2010 *Nature* **465** 901
[3] Heinze S, von Bergmann K, Menzel M, Brede J, Kubetzka A, Wiesendanger R, Bihlmayer G and Blugel S 2010 *Nature* **7** 713
[4] Nagaosa N and Tokura Y 2010 *Nat. Nanotechnol.* **8** 899
[5] Zhang X C, Zhou Y, Song K M, Park T E, Xia J, Ezawa M, Liu X X, Zhao W S, Zhao G P and Woo S 2020 *J. Phys.: Condens. Matter* **32** 143001
[6] Fert A, Cros V and Sampaio J 2013 *Nat. Nanotechnol.* **8** 152
[7] Sampaio J, Cros V, Rohart S, Thiaville A and Fert A 2013 *Nat. Nanotechnol.* **8** 839
[8] Iwassaki J, Mochizuki M and Nagaosa N 2013 *Nat. Commun.* **4** 1463
[9] Mochizuki M 2012 *Phys. Rev. Lett.* **108** 017601
[10] Onose Y, Okamura Y, Seki S, Ishiwata S and Tokura Y 2012 *Phys. Rev. Lett.* **109** 037603
[11] Lin S Z, Batista C D and Saxena A 2012 *Phys. Rev. B* **89** 024415
[12] Zhang X, Zhao G P, Fangohr H, Liu J P, Xia J and Morvan F J 2015 *Sci. Rep.* **5** 7643
[13] Yoo M W, Cros V and Von Kim J 2017 *Phys. Rev. B* **95** 184423
[14] Zhang X, Zhou Y and Ezawa M 2016 *Nat. Commun.* **7** 10293
[15] Upadhyaya P, Yu G, Amiri P K and Wang K L 2015 *Phys. Rev. B* **92** 134411
[16] Fook H, Gan W, Purnama I and Lew W 2015 *IEEE Trans.* **51** 1500204
[17] Purnama I, Gan W, Wong D and Lew W 2015 *Sci. Rep.* **5** 10620
[18] Lai P, Zhao G, Tang H, Ran N, Wu S, Xia J, Zhang X and Zhou Y 2017 *Sci. Rep.* **7** 45330
[19] Mulkers J, Van Waeyenberge B and Milosevic M V 2017 *Phys. Rev. B* **95** 144401
[20] Zhang Y, Luo S, Yan B, Ou-Yang J, Yang X, Chen S, Zhu B and You L 2017 *Nanoscale* **9** 10212
[21] Xing X, Akerman J and Zhou Y 2020 *Phys. Rev. B* **101** 214432
[22] Zhang X, Zhou Y and Ezawa M 2016 *Nat. Commun.* **7** 10293
[23] Barker J and Tretiakov O A 2016 *Phys. Rev. Lett.* **116** 147203
[24] Zhang X, Zhou Y and Ezawa M 2016 *Sci. Rep.* **116** 24795
[25] Zhang X C, Xia J, Zhou Y, Wang D W, Liu X X, Zhao W S and Ezawa M 2016 *Phys. Rev. B* **94** 094420
[26] Zazvorka J, Jakobs F, Heinze D, Keil N, Kromin S, Jaiswal S, Litzius K, Jakob G, Virnau P, Pinna D, Eversechor-Sitte K, Rozsa L, Donges A, Nowak U and Klaui M 2019 *Nat. Nanotechnol.* **14** 658
[27] Tan A, Ho P, Pin L, James H, Lisen T, Khume R, Cynthia R, Charles S and Anjan S 2021 *Nat. Commun.* **12** 4252
[28] Kolesnikov A G, Stebliy M E, Samardak A S and Ognev A V 2018 *Sci. Rep.* **8** 16966
[29] Wang X F, Wang X S, Wang C, Yang H H, Cao Y S and Yan P 2019 *J. Phys. D: Appl. Phys.* **52** 225001
[30] Xin M and Liu Y 2021 *J. Magn. Magn. Mater.* **536** 168142
[31] Lin S, Charles R B, Cristian D and Saxena A 2013 *Phys. Rev. Lett.* **110** 207202
[32] Vansteenkiste A, Leliaert J, Dvornik M, Helsen M, Garcia-Sanchez F and Waeyenberge F B V 2014 *AIP Adv.* **4** 107133
[33] Wang W, Albert M, Beg M, Bisotti M A, Chernyshenko D, Cortés-Ortuño D, Hawke I and Fangohr H 2015 *Phys. Rev. Lett.* **114** 087203
[34] Venkat G, Fangohr H and Prabhakar A 2018 *J. Magn. Magn. Mater.* **450** 34
[35] Papanicolaou N and Tomaras T N 1991 *Nucl. Phys.* **360** 425
[36] Ishida Y and Kondo K 2020 *J. Magn. Magn. Mater.* **493** 165687
[37] Kong L and Zang J 2013 *Phys. Rev. Lett.* **111** 067203
[38] Qiu L, Xia J, Feng Y, Shen L, Morvan F J, Zhang X, Liu X, Xie L, Zhou Y and Zhao G 2020 *J. Magn. Magn. Mater.* **496** 165922